Electronic Supplementary Material (ESI) for Journal of Materials Chemistry C.

Supporting Information

Photovoltaic Memristor based on Photoelectric Synaptic Plasticity of Bulk Photovoltaic Effect

Yang Chen, Haoming Wei, Yangqing Wu, Tengzhou Yang, Bingqiang Cao**

1.Bulk photovoltaic memristor characteristics

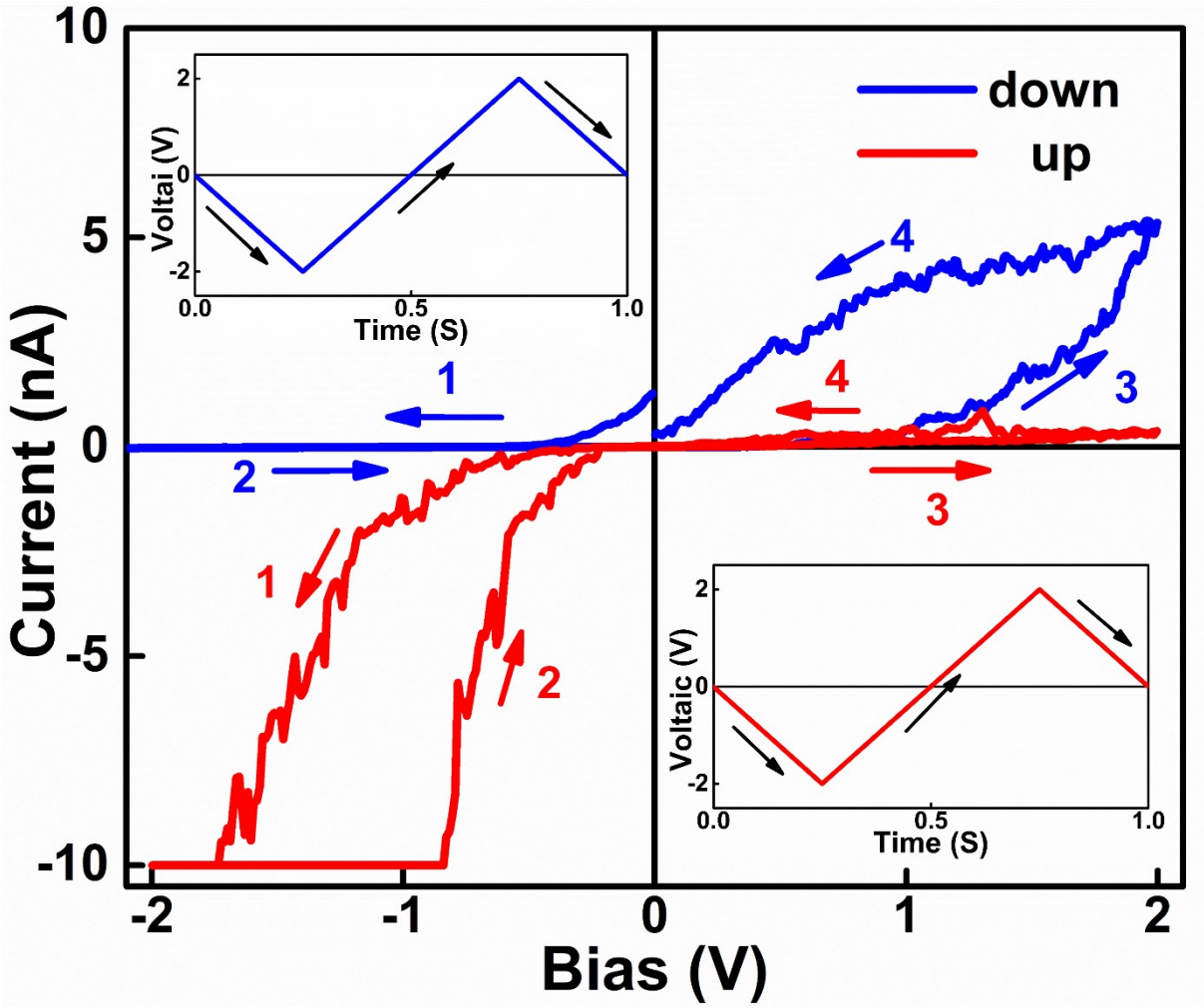

Figure S1. *I-V* characteristics curves of BFO device with downward and upward polarization directions.

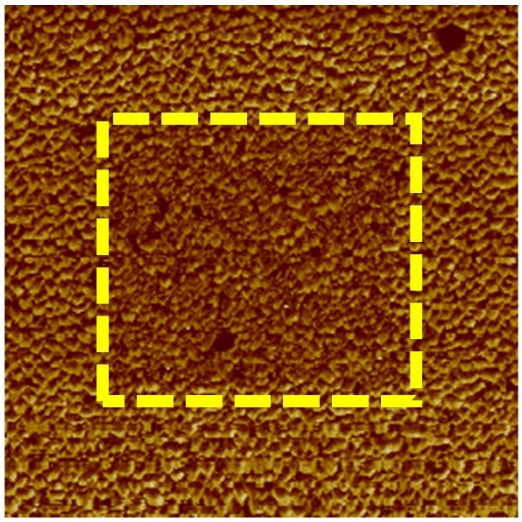

Figure S2. Corresponding out-of-plane PFM phase images of the BFO film with switched box-in-box patterns.

In this section, PFM is used to pre-polarize BFO films to explore the single direction conduction properties of memristors in two polarization directions. The polarized upward film preserves the intrinsic polarization state of the film and the polarized downward film is scanned by the PFM probe applying -2 V voltage. In addition, we started the test from 0 V, which is conducive to releasing the polarized charge in advance and reducing the test frequency to prevent repeated AC signals from charging and discharging the device. In Figure S1, when the polarization direction is downward, the device is on state only in the positive (0 ~ 0.5 S) sweep voltage. When the polarization direction is upward, the device is on state only in the negative (0 ~ 0.5 S) sweep voltage. The results show that the memristor properties of BFO films are closely related to the polarization direction of ferroelectric domains. The Figure S2 shows the out-of-plane PFM amplitude images of the BFO film with switched box-in-box patterns.

2. The measurement of domain switching

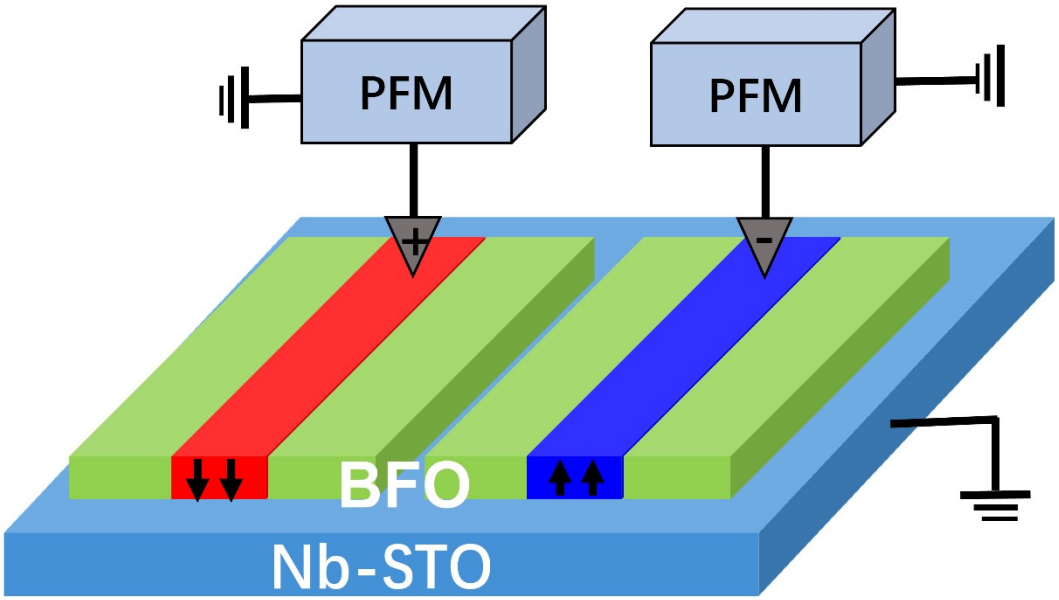

Figure S3. The Schematic diagram of polarization writing (a)down and (b) up by PFM**.**

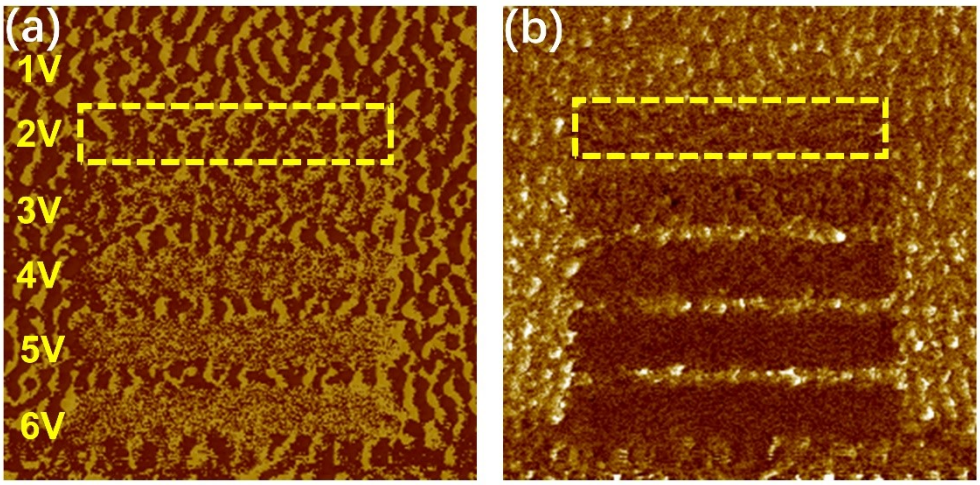

Figure S4. Evolution of PFM in-plane (a) phase and (b) amplitude switching images under different bias voltage.

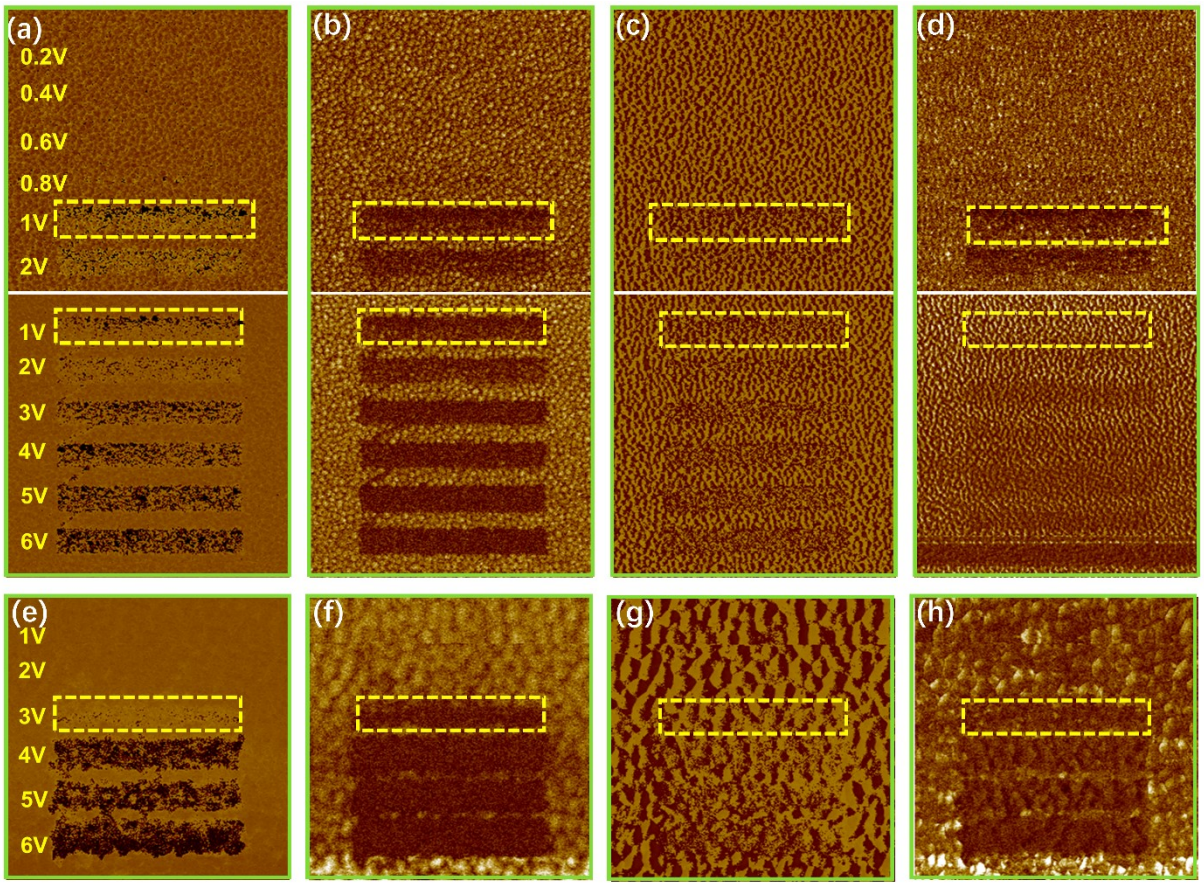

Figure S5. The out-of-plane PFM (a) phase and (b) amplitude switching images of 40nm BFO film under different bias voltage of tip. The in-plane PFM (c) phase and (d) amplitude switching images of 40 nm BFO film under different bias voltage of tip. The out-of-plane PFM (e) phase and (f) amplitude switching images of 170 nm BFO film under different bias voltage of tip. The in-plane PFM (g) phase and (h) amplitude switching images of 170 nm BFO film under different bias voltage of tip.

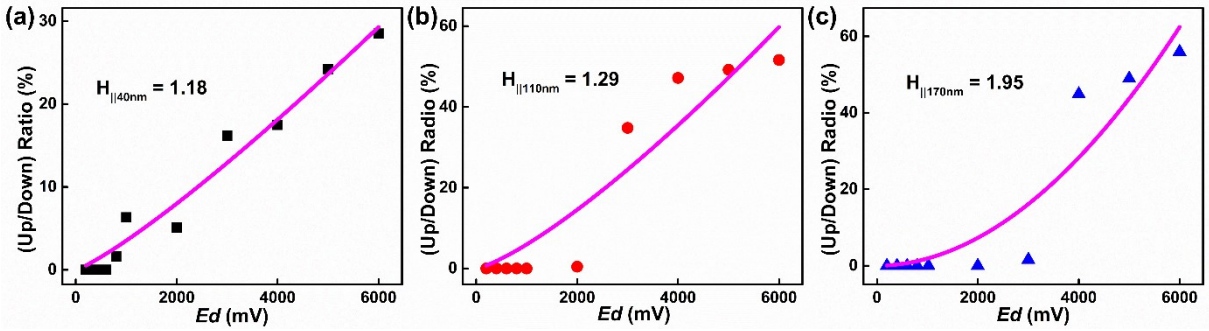

Figure S6. Normalized switched area as a function of switching pulse voltages. The pink lines are fit results from Landau-Lifshiz-Kittel scaling power law. The domain switching ratio of (a) 40 nm, (b) 110 nm and (c) 170nm films versus electric fields for out-of-plane.

In this section, as shown in Figure S5, different thickness BFO films were polarized by PFM tips bias to investigate the switching kinetics of domain. Figure S5 shows that domains begin to change the polarization from up (bright domains) to down (down domains) when the electric field intensity reaches the switching threshold. With the increase of bias voltage, the domain reverse more and more completely. We study the switching dynamics of domains under different electric fields by counting the ratio of polarized upward and polarized downward domains.

3. Synaptic plasticity in transverse devices

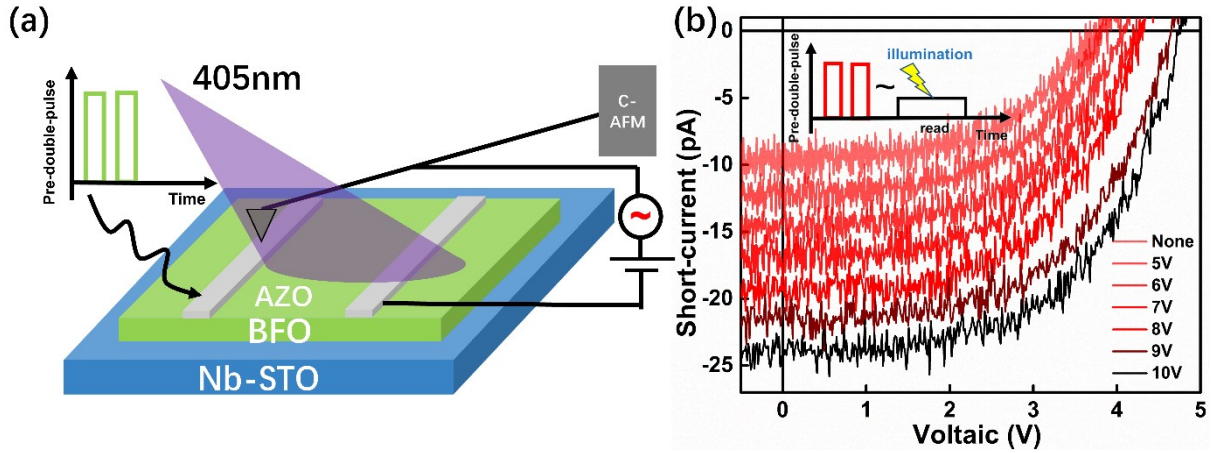

Figure S7 (a) The Schematic diagram of lateral photovoltaic synaptic memristor structure with C-AFM. (b) The photovoltaic *I–V* characteristics curves of lateral memristor recorded after different amplitudes of Pre-DP voltages.

In this part, the AZO electrodes are set on the upper surface of BFO film at a distance of 500 μm as shown in Figure S7a. As the electrode distance increases, the depolarization field between the electrodes increases, which greatly increases the V_{oc} of BPVE. The lateral device lacks the connection of highly conductive "folded curtain" domain walls, with an I_{sc} of only 10 pA. The lateral PVM also shows photovoltaic synaptic plasticity under PPF, with V_{oc} increasing from 3.5 V to 4.5 V and I_{sc} increasing from 10 pA to 25 pA. However, due to the low plasticity of in-plane domain, the synaptic plasticity of lateral device is significantly lower than that of vertical ones.

4. Photovoltaic plasticity under single pulse

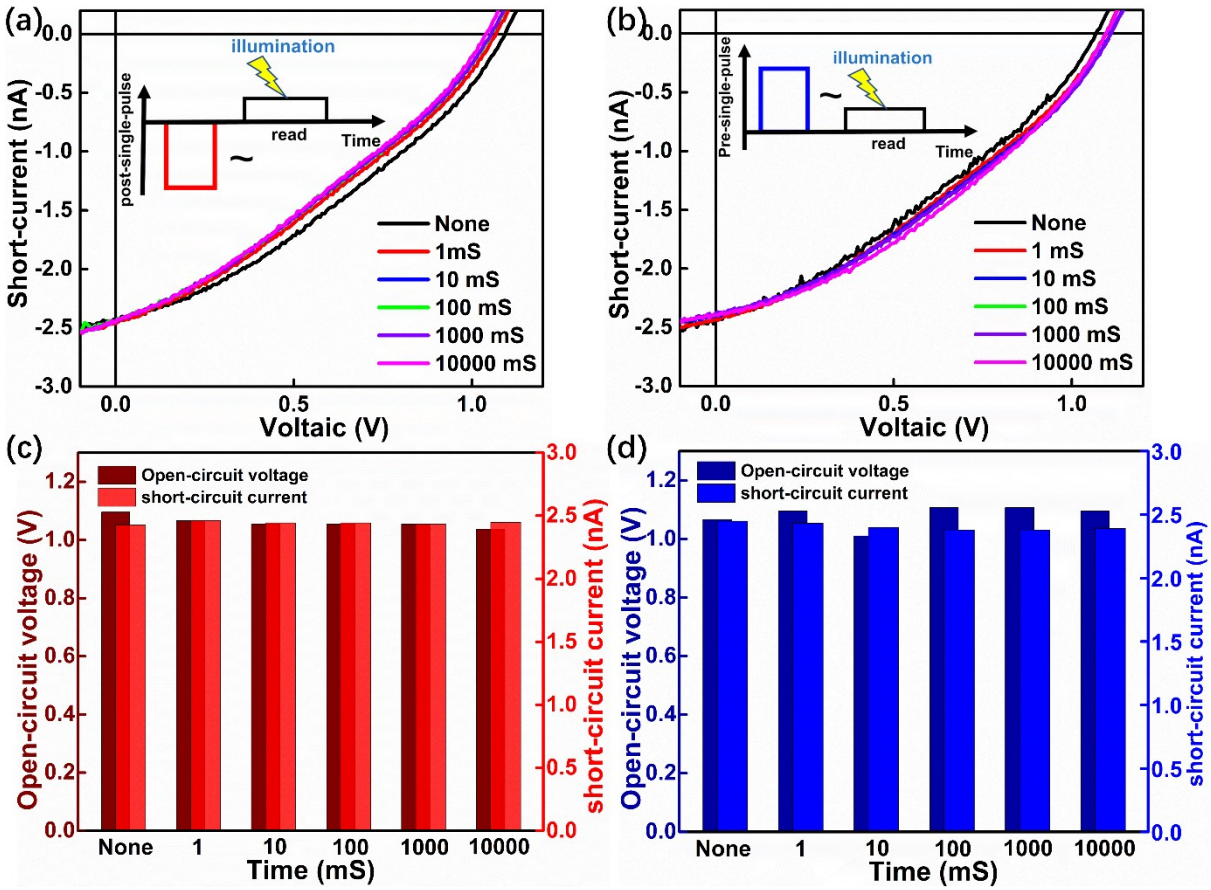

Figure S8. The photovoltaic *I–V* characteristics curves of PVM recorded after different durations of (a) Post-SP and (b) Pre-SP pulse voltages. The inset is schematic diagram of pulse write voltages and read operating voltage. The V_{oc} and I_{sc} of memristor recorded after different durations of (c) Post-SP and (d) Pre-SP pulse voltages.

In this section, Post-SP and Pre-SP voltages with amplitudes of 2 V for different durations are written to the memristor as shown in Figure S8. The results show that neither erasure nor write processes achieve changes in synaptic photovoltaic weight at single pulse voltage. This may be due to some unique pinning effect of ferroelectric domains that prevents continuous voltage input from causing continuous rotation in the direction of domain polarization.

5. Characterization of optical properties.

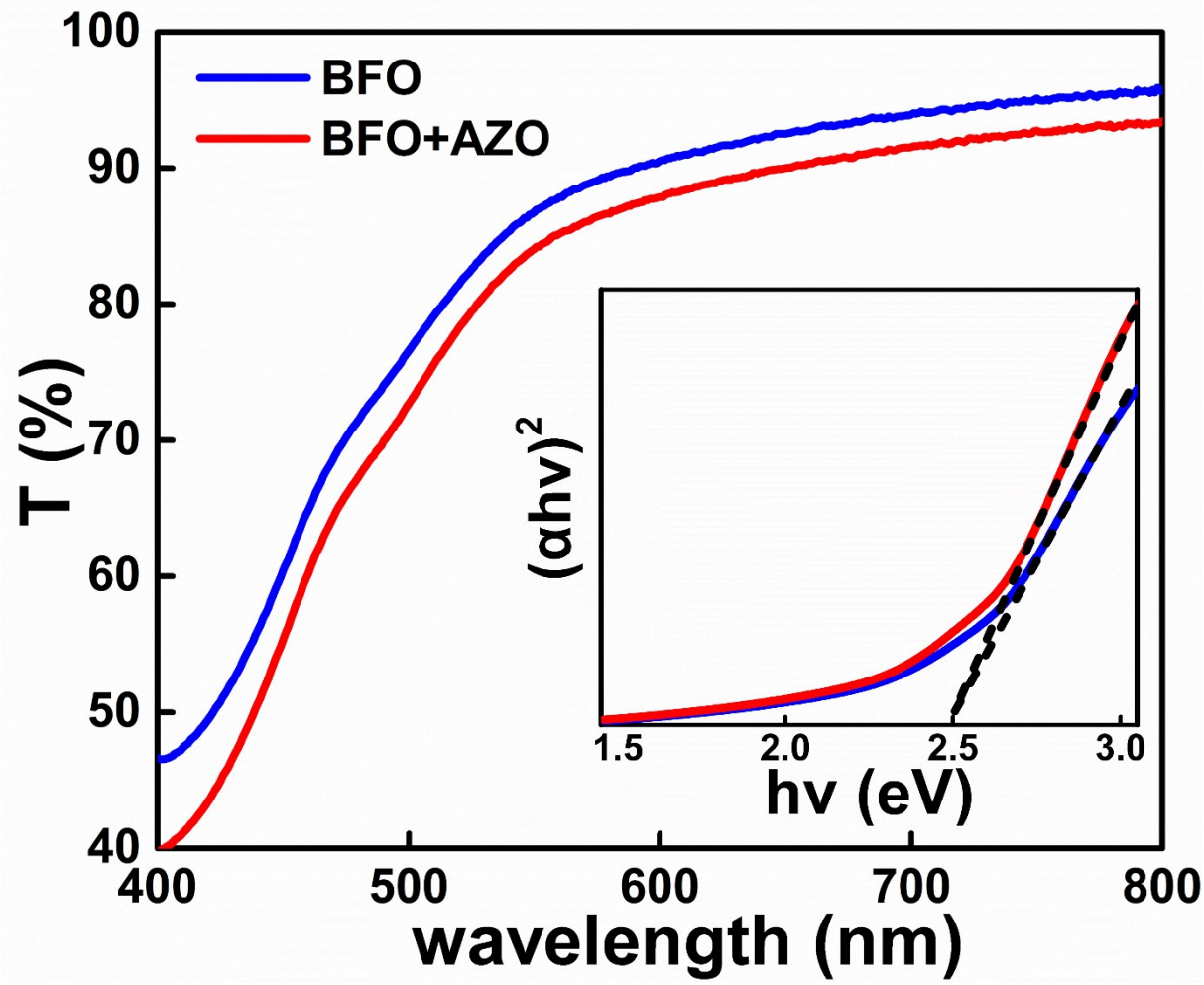

Figure S9. UV transmission spectrum of the BFO and BFO/AZO films with the inset showing the Tauc plot.

In this section, the transmission spectra of BFO film and BFO/AZO film were shown in Figure S10. The results show that AZO top electrode has high transmission and does not affect the illumination radiation absorption of BFO layer. To study the optical bandgap of films, the Tauc relationship was employed: $^{\alpha h\nu \propto (h\nu - E_g)^n}$. With n = 1/2 for (direct-allowed), the band gap of BFO device is calculated to be about 2.5 eV. Therefore, 405 laser can be used as an illumination source to stimulate the BPVE in BFO device.

6. The measurement of the spatially resolved photovoltaic current distribution mapping

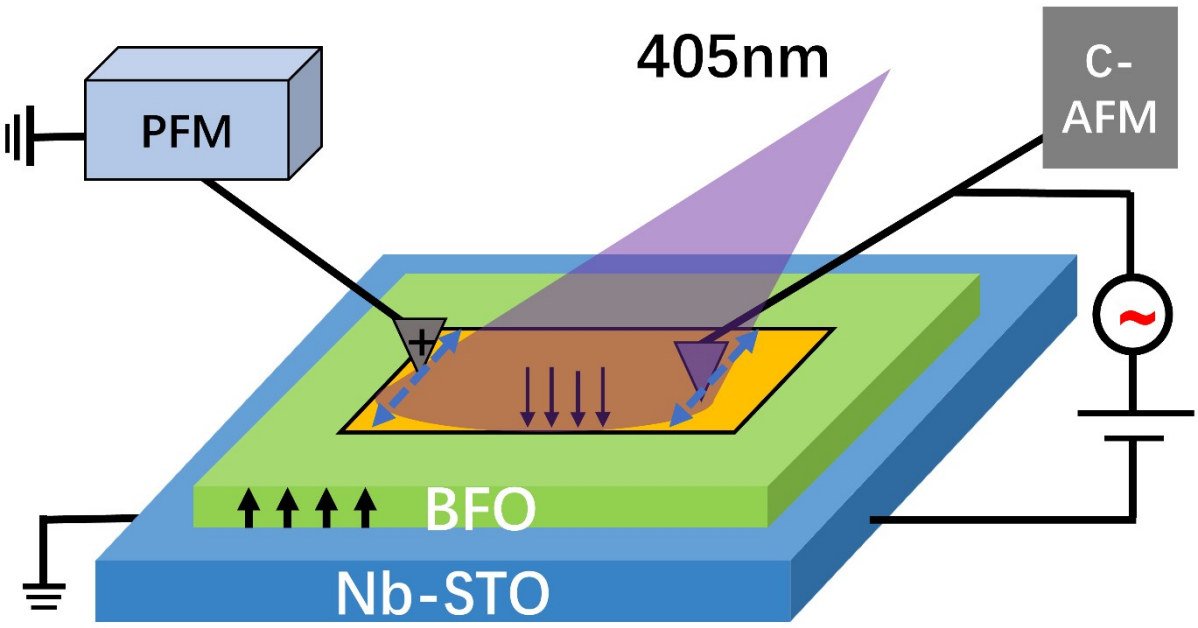

Figure S10. The Schematic diagram of the spatially resolved photovoltaic current distribution mapping by C-AFM

Under the illumination , the probe of the PFM and C-AFM directly scans the surface of the film using contact mode and can measure the photocurrent on the film surface in real time to produce a spatially resolved photocurrent mapping as shown in **Figure S10**.